Development of a Very Low-Noise Cryogenic Preamplifier for Large-Area SiPM Devices

Marco D'Incecco, Cristiano Galbiati, Graham K. Giovanetti, George Korga, Xinran Li, Andrea Mandarano, Alessandro Razeto, Davide Sablone, and Claudio Savarese

Abstract—Silicon photomultipliers (SiPMs) are an excellent candidate for the development of large-area light sensors. Large SiPM-based detectors require low-noise preamplifiers to maximize the signal coupling between the sensor and the read-out electronics. This paper reports on the development of a low-noise transimpedance amplifier sensitive to single-photon signals at cryogenic temperature. The amplifier is used to read-out a 1-cm² SiPM with a signal-to-noise ratio in excess of 40.

Index Terms—Cryogenic electronics, low-noise amplifier, silicon-germanium (SiGe), silicon photomultipliers (SiPMs), transimpedance amplifier (TIA).

I. INTRODUCTION

THE improvements in performance of silicon photomultipliers (SiPMs) at cryogenic temperature [1] and the availability of low-noise heterojunction amplifiers open the door to the development of cryogenic, large-area, SiPM-based photodetectors as replacements for the photomultiplier tubes. We introduce and describe a low-noise transimpedance amplifier (TIA) designed to instrument large-area assemblies of SiPMs intended for operation at cryogenic temperature. As the scale and sensitivity of rare-event physics searches grows, so does the need for large-, high-efficiency light detectors. These amplifiers were designed for use in the DarkSide-20k dark matter detector, which will instrument an active volume of about 23t of liquid argon with 14 m² of SiPMs [2]. Due to their excellent signal-to-noise performance, they are also

Manuscript received November 14, 2017; accepted January 24, 2018. Date of publication January 29, 2018; date of current version April 12, 2018. This work was supported in part by NSF, USA, under Grant PHY-1314507, in part by the Istituto Nazionale di Fisica Nucleare, Italy, in part by the Laboratori Nazionali del Gran Sasso, INFN, Italy, and in part by the Fermilab, Department of Energy, under Contract DE-AC02-07CH11359. (Corresponding author: Claudio Savarese.)

- M. D'Incecco is with the Laboratori Nazionali del Gran Sasso, Istituto Nazionale di Fisica Nucleare, 67100 Assergi, Italy.
- C. Galbiati, G. K. Giovanetti, and X. Li are with the Physics Department, Princeton University, Princeton, NJ 08544 USA.
- G. Korga is with Department of Physics, University of Houston, Houston, TX 77204 USA, and also with the Laboratori Nazionali del Gran Sasso, Istituto Nazionale di Fisica Nucleare, 67100 Assergi, Italy.
- A. Mandarano and C. Savarese are with the Gran Sasso Science Institute, 67100 L'Aquila, Italy, and also with the Laboratori Nazionali del Gran Sasso, Istituto Nazionale di Fisica Nucleare, 67100 Assergi, Italy (e-mail: claudio.savarese@gssi.infn.it).
- A. Razeto and D. Sablone are with the Laboratori Nazionali del Gran Sasso, Istituto Nazionale di Fisica Nucleare, 67100 Assergi, Italy, and also with the Physics Department, Princeton University, Princeton, NJ 08544 USA.

Color versions of one or more of the figures in this paper are available online at http://ieeexplore.ieee.org.

Digital Object Identifier 10.1109/TNS.2018.2799325

generally used as a building block for realization of other large SiPM assemblies.

Development of the amplifier was done in a dedicated cryogenic setup, consisting of a Cryomech PT90 pulse tube cryocooler mounted on the top flange of a stainless steel cryostat evacuated to 10^{-2} mbar. The cryocooler cold finger extends into the cryostat and holds the devices under test. The temperature of the cold finger is monitored by a set of platinum resistance temperature detector and regulated by a Lakeshore 335 to within 1 K of a set-point temperature. The setup is capable of operating within the range from 40 to 300 K.

The core of the TIA is an LMH6629 high-speed operational amplifier from Texas Instruments. The cryogenic characterization of the LMH6629 will be described in Section II. The characteristics of the SiPMs used for testing, the design of the TIA, and the analysis algorithms will be discussed in Section III. Finally, the results of the read-out of a 1-cm² SiPM will be described in Section IV.

II. LMH6629 CHARACTERIZATION

The performance of the standard silicon bipolar junction transistors degrades at cryogenic temperatures [3], whereas that of the heterojunction bipolar transistors (HBT) does not, making HBTs as an interesting alternative to CMOS technology for the cryogenic applications. An HBT is a type of bipolar junction transistor that uses different semiconductor materials for the emitter and base regions. Among the available technologies, silicon–germanium (SiGe) HBTs, which are manufactured by many foundries for high-bandwidth applications, are particularly well suited for cryogenic operation because of their bandgap-engineered base [4].

The LMH6629 is a high-speed, ultralow-noise amplifier fabricated with SiGe technology by Texas Instruments. The device is designed for applications requiring a wide bandwidth with high gain and low noise [5]. The amplifier is available in two packages: a standard SOT-23-5 and a lead-less WSON-8. The WSON-8 package has selectable internal compensation for operation at low gains. Without this additional compensation enabled, the amplifier is stable only for gains larger than 10 V/V at cryogenic temperatures. This paper focuses on the WSON-8 package, which was selected, because its die attach pad improves thermalization.

Measurements of the LMH6629 were performed on custom FR4 printed circuit boards installed on the cold finger of the

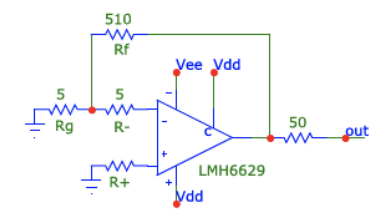


Fig. 1. Schematic of the circuit used to measure the intrinsic noise sources of the LMH6629.

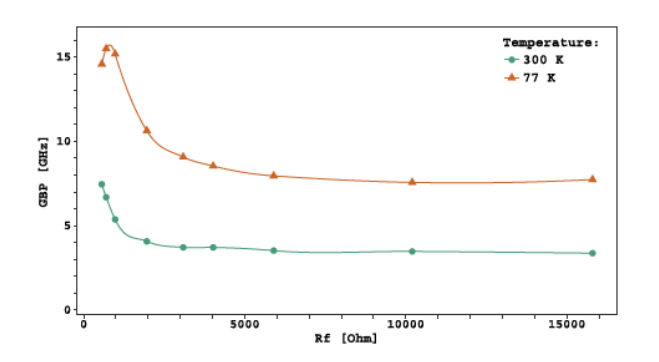


Fig. 2. GBP of the LMH6629 test circuit in the noninverting configuration versus feedback resistor value ($R_g = 50~\Omega, 5~V$). The LMH6629 is operated with the reduced internal compensation enabled. The lines are drawn to guide the eye.

cryogenic setup. The passive components in the circuit were carefully selected for their cryogenic compatibility. All of the capacitors in the circuit are either COG/NPO or PPS [6], and the resistors are based on a thin or thick metal film.

A. Bandwidth

The measurement of the intrinsic bandwidth of the LMH6629 is complicated by parasitic effects from the circuit in which the chip is operated. In fact, a small capacitance on the feedback path can significantly reduce the measured bandwidth. Such behavior is shown in Fig. 2, where the gain bandwidth product (GBP) of the test circuit is shown for different feedback resistor (R_f) values. The GPB rapidly decreases as R_f increases, eventually reaching a plateau. The spice simulation described in Section II-F models this effect by including a 0.2-pF feedback parasitic capacitance (C_f) .

The GBP was measured by extracting the noise gain and the frequency of the half-power point ($F_{-3~dB}$) from spectra collected with an Agilent model 5071c vector network analyzer (VNA) configured for S_{21} scans. Fig. 3 shows the GBP temperature dependence measured in both the inverting and noninverting configurations ($R_f = 1~\mathrm{k}\Omega$). The GBP of the amplifier is exponential with temperature as shown by the fit in Fig. 3. When operated with a 3-V power supply, the amplifier performance quickly degrades below 160 K.

B. Input Bias Current

The input bias current (i_b) of the LMH6629 was determined using the circuit shown in Fig. 1 with $R_+=620~\Omega$. The dc output of the circuit is given by $i_b\left(R_+-(R_-+R_g\parallel R_f)\right)G$, with $G=R_f/R_g+1$. The results of the measurement

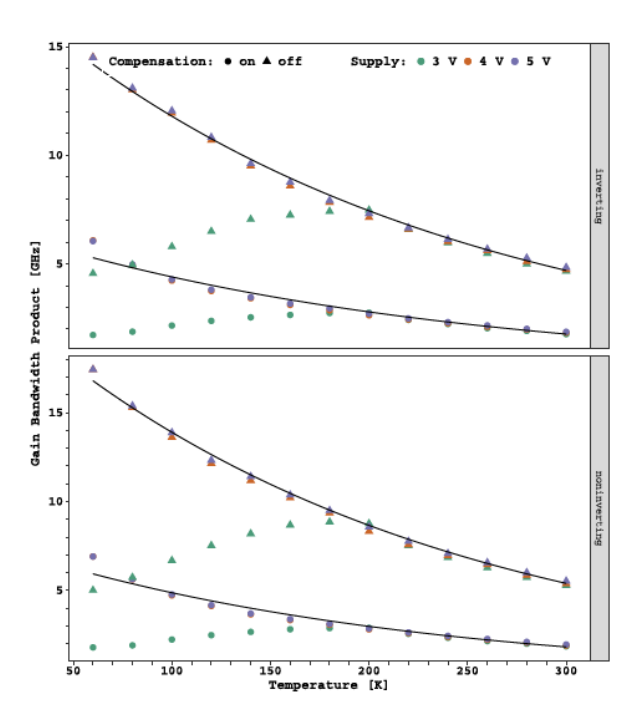


Fig. 3. GBP of the LMH6629 circuit with $R_f=1~\mathrm{k}\Omega$ in inverting and noninverting configurations versus temperature. The black lines correspond to exponential fits.

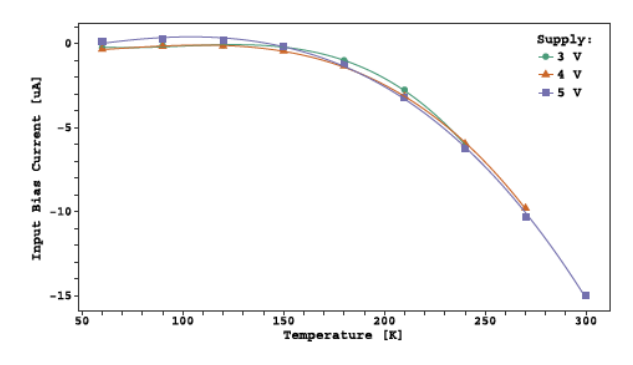


Fig. 4. Input bias current of the LMH6629 versus temperature with different power supply voltages. The lines are drawn to guide the eye.

are shown in Fig. 4. At room temperature, $i_b = -15~\mu\text{A}$, in agreement with the value reported on the datasheet. It is interesting to note that the input bias current rapidly decreases at low temperature, reaching a plateau of about $\pm 1~\mu\text{A}$ at about 150 K.

C. Input Noise

Measurements of the voltage (e_n) and current (i_n) noise terms as a function of temperature were done with the LMH6629 configured as shown in Fig. 1. The amplifier output was acquired with an R&S FSV 7 spectrum analyzer and an R&S RTO1024 oscilloscope operating as a spectrum analyzer. The output noise density was determined at 1 MHz in a flat region of the power spectra, far from any environmental noise pickup and the half-power point. Fig. 5 shows the results for several values of R_+ along with fits to the noise model described later in this paper.

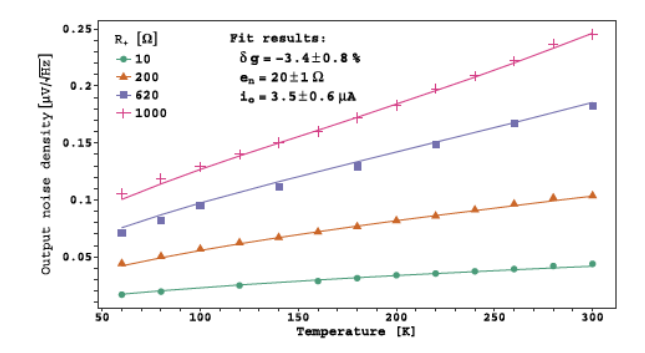


Fig. 5. Output noise density at 1 MHz of the circuit shown in Fig. 1 operated at 4 V versus temperature. Solid line: best fit to the data of the model described in the text.

The output noise density (N_o) as a function of temperature (T) can be expressed as

$$N_o = \frac{G}{2} \sqrt{4k_B T R_{eq}^J + e_n^2(T) + i_n^2(T) R_i^2}$$
 (1)

where k_B is the Boltzmann's constant

$$\begin{split} R^{J}_{eq} &= R_{+} + R_{-}^{*} \xi^{2}, \quad R^{2}_{i} = R_{+}^{2} + R_{-}^{*2} \xi^{2} \\ \xi &= (G-1)/G, \quad \text{and} \ R_{-}^{*} = R_{f} \parallel R_{g} + R_{-}. \end{split}$$

Equation (1) accounts for the Johnson-Nyquist noise of the resistors in the circuit and for the intrinsic noise sources of the LMH6629.

The fit model assumes that $e_n(T)$ behaves like the Johnson–Nyquist noise source with resistance $R_n(e_n(T) = (4 k_B T R_n))^{1/2}$ and that $i_n(T)$ is due to the shot noise of the input current $[i_n = (2 e^-(|i_b(t)| + |i_o|))^{1/2}$ with the input bias current, $i_b(T)$, measured in Section II-B and i_o assumed constant]. The best fit values are as follows.

- $R_n = (25 \pm 1) \Omega$, which at 300 K is equivalent to $(0.64 \pm 0.01) \text{ nV}/\sqrt{\text{Hz}}$, compared to 0.69 $\text{nV}/\sqrt{\text{Hz}}$ on the datasheet.
- $i_o = (3.5 \pm 0.6) \mu A$, for a total shot noise density of $(2.4 \pm 0.1) \text{ pA}/\sqrt{\text{Hz}}$, compared to 2.6 pA/ $\sqrt{\text{Hz}}$ on the datasheet.
- $\delta G = (-3.4 \pm 0.8 \%)$, where δG is the relative variation of the gain with respect to the theoretical value and is allowed to float during the fit.

Overall, the experimental values are well described by the model. The standard deviation of the relative residuals is 2.5%, mostly due to the measurements performed with large R_+ values. This indicates that the accuracy of the scaling model of the current noise with temperature needs to be improved. However, in this paper, i_n has no effect on the overall noise budget given the small value of the resistors in use (see Section III-C).

D. Dynamic Range

The dynamic range of the LMH6629 output was measured using the VNA configured for a power sweep at 1 MHz in S_{21} mode. Fig. 6 shows the 1-dB compression point as a function of temperature for two different power supply voltages (4 and 5 V) along with a linear fit to the data. Fig. 6 plots the peak-to-peak voltage. When the circuit is used as a pulse amplifier, the effective dynamic range is halved.

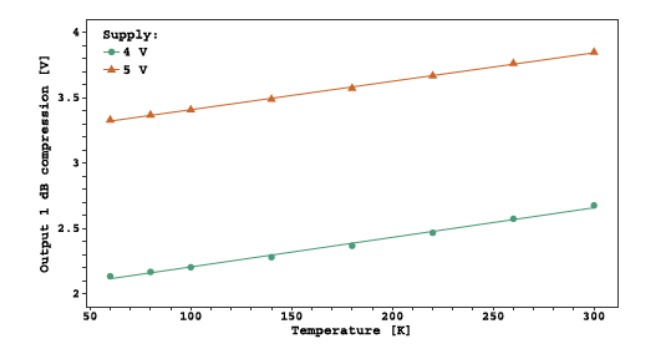


Fig. 6. Peak-to-peak output compression (1 dB) of the LMH6629 versus temperature. The lines represent a linear fit to the data.

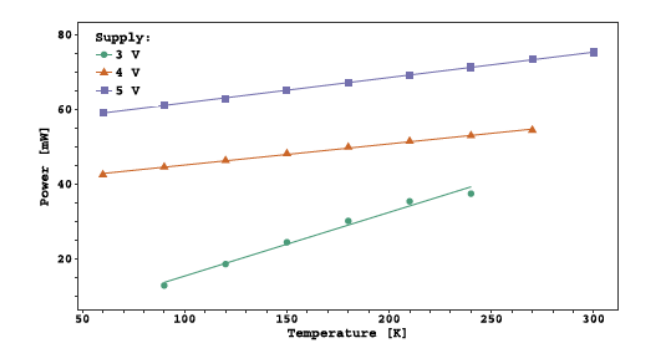


Fig. 7. Power consumption of the LMH6629 versus temperature. The lines represent a linear fit to the data.

E. Power Consumption

The power consumption of the LMH6629 was estimated by measuring the current flowing in the circuit when no load was connected to the output. Fig. 7 shows the results for various supply voltages along with a linear fit to the data.

F. Simulation

Texas Instruments provides a SPICE model of the LMH6629 that was verified with Microcap 10 from Spectrum Software. While the noise simulation is accurate at better than a few percent within the temperature range of interest, the simulated bandwidth does not follow the experimental behavior of the amplifier, consistently predicting a smaller GBP than what was measured (up to a factor of more than 2) for temperatures below 270 K.

III. TRANSIMPEDANCE AMPLIFIER

Based on the performance of the LMH6629, a low-noise TIA was designed for the cryogenic applications.

A. NUV-HD-LF SiPM

The TIA was optimized for use with a custom batch of near ultra violet-high density-low field (NUV-HD-LF), $10 \times 10 \text{ mm}^2$ area SiPMs produced by Fondazione Bruno Kessler (FBK) for DarkSide-20k [2]. These devices are similar to FBK's standard 25 $-\mu$ m NUV-HD technology [7] but are engineered to have a lower field strength in the

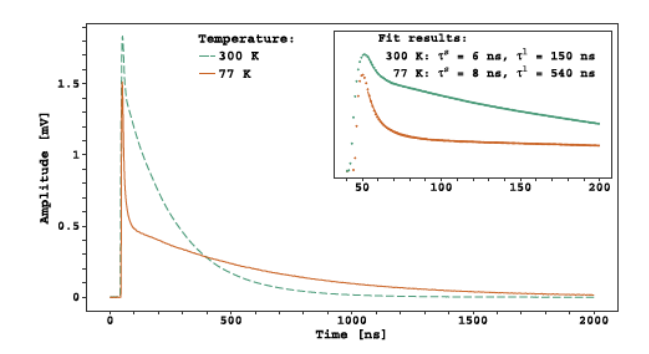


Fig. 8. Average waveform of a NUV-HD-LF $10 \times 10 \text{ mm}^2$ SiPM photoelectron acquired with the TIA described in the text with $R_f = 2 \text{ k}\Omega$ and $R_s = 20 \Omega$. Inset: zoommed-in view of the fast peak (points) and the fit with a double exponential (solid lines); the rise time is about 2 ns, read-out limited.

TABLE I $R_d \ \ {\rm AND} \ C_d \ \ {\rm Values} \ \ {\rm for} \ \ 10 \times 10 \ {\rm mm}^2 \ \ {\rm NUV\text{-}HD\text{-}LF}$ SIPM at Breakdown Voltage

Frequency	R_d^{300K} $[\Omega\mathrm{cm}^2]$	C_d^{300K} [nF/cm ²]	R_d^{77K} $[\Omega\mathrm{cm}^2]$	C_d^{77K} [nF/cm ²]
$10\mathrm{kHz}$	35	6.3	74	6.7
$100\mathrm{kHz}$	14	6.2	63	6.6
$200\mathrm{kHz}$	13	6.2	63	6.5
$500\mathrm{kHz}$	12	6.1	62	5.8
$1\mathrm{MHz}$	11	5.9	61	4.2

All measures have an uncertainty of 1 unit on the last digit.

avalanche region [8] and a smaller quenching resistance ($R_q=2.2~\mathrm{M}\Omega$ at room temperature) to provide a relatively fast signal. The average photoelectron signal from a NUV-HD-LF $10\times10~\mathrm{mm}^2$ SiPM is shown in Fig. 8, both at room and liquid-nitrogen temperature. These SiPMs can be operated in liquid nitrogen with gains up to $1.5\times6~\mathrm{C/C}$. In this paper, the SiPM operating voltage is tuned so that at each operating temperature, the gain remains stable at $1\times6~\mathrm{C/C}$.

The recharge time constant of the SiPM was determined over the interval 60-300 ns by a fit to the formula

$$\tau^l = \tau_0 / T^a \tag{2}$$

where $\alpha = 1.04 \pm 0.01$ and $\tau_0 = (51 \pm 3)$ with a standard deviation of the relative residuals of 2%.

In addition to the characteristics of the NUV-HD-LF SiPMs reported in [1], the detector equivalent capacitance (C_d) and its equivalent series resistance (R_d) are relevant for this paper. As discussed in [9], these parameters are the result of the summing of all the microcell properties: resistance of the quenching resistor (R_q) , capacitance of the quenching resistor (C_q) , and the cell intrinsic capacitance (C_{SPAD}) . The characterization of the microcell properties at cryogenic temperatures is beyond the scope of this paper. A direct measurement of C_d and R_d was done using an Agilent E4980A RLC meter and the results are reported in Table I.

Some observations can be made from the measurement of C_d and R_d . First, while the detector capacitance remains

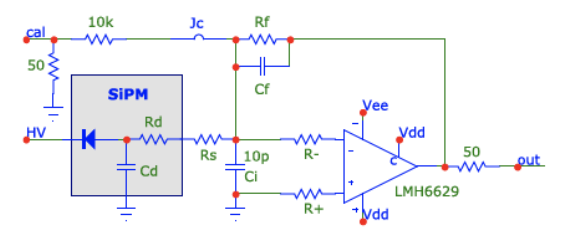


Fig. 9. Schematic of the TIA described in the text. During regular operation, the calibration input is disconnected (at J_c) to avoid injecting noise: the 10-k Ω resistor ensures that the calibration input behaves as a current like source.

relatively constant with temperature variation, R_d increases in liquid nitrogen by about a factor of 5. This is due to the large variation of R_q , which is a poly-silicon resistor. This in turn increases the SiPM recharge time. Second, both R_d and C_d vary as a function of frequency. To first order, R_q , C_q , and $C_{\rm SPAD}$ form a filter network with one pole in $Fp=R_q\times C_q$, which at room temperature has a value in the range 10–20 MHz (see [9]). For higher frequencies, R_d asymptotically approaches zero. At cryogenic temperature, the larger value of R_q shifts the pole down to a few MHz. By assuming a ratio $C_{\rm SPAD}/C_q\simeq 10$, Fp can be estimated as $(1/(2\pi\,Rd\,Cd/10))$ corresponding to 18 MHz at room temperature and 4 MHz at 77 K.

B. Preamplifier Design

The schematic of the TIA is shown in Fig. 9. The circuit is based on an LMH6629 operating with a 4-V supply voltage and its on-chip compensation reduced.

The resistors R_- and R_+ (both 10 Ω) at the inverting and noninverting inputs are required to avoid high-frequency oscillations at cryogenic temperature. This is done at the cost of a roughly 20% increase in the voltage noise, e_n . The 10-pF capacitor C_i minimizes undershoot due to the fast discharge of the SiPM. The feedback capacitance, C_f , is only a few hundreds of fF and is due to the stray capacitance of the printed circuit board, as discussed in Section II-A.

The series resistor, R_s (and to some extent R_d), plays an important role in the performance of the amplifier. For frequencies above $F_l = (1/(2\pi C_d(R_s + R_d)))$, the system behaves like an inverting amplifier due to the presence of R_s and R_d . This means that the bandwidth is proportional to the GBP of the amplifier, in contrast to an ideal TIA, where the bandwidth scales as the square root of the GBP. The result is an increased bandwidth. Fig. 10 shows the temperature scaling of the preamplifier bandwidth as measured by S_{21} VNA scans between the calibration input and the output with the SiPM connected. In addition, the series resistor changes the noise gain so that, for frequencies above F_l , it plateaus at $N_g = (R_f/(R_s + R_d + 1))$. This in turn reduces the output noise without changing the transfer function for current sources, such as SiPMs.

However, large values of R_s will alter the output signal shape by creating a low-pass filter with the detector capacitance and, more importantly, significantly contribute to the noise budget.

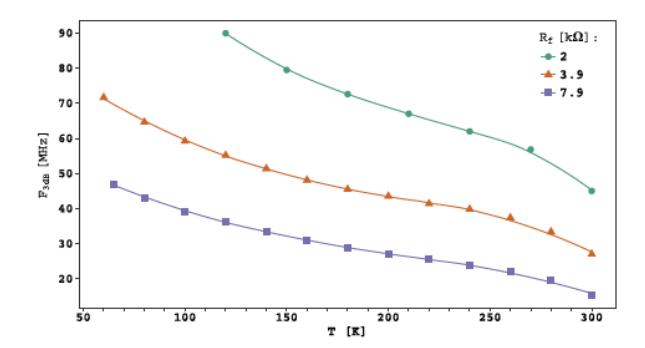


Fig. 10. $F_{-3~\mathrm{dB}}$ of the TIA discussed in the text. The lines are drawn to guide the eye.

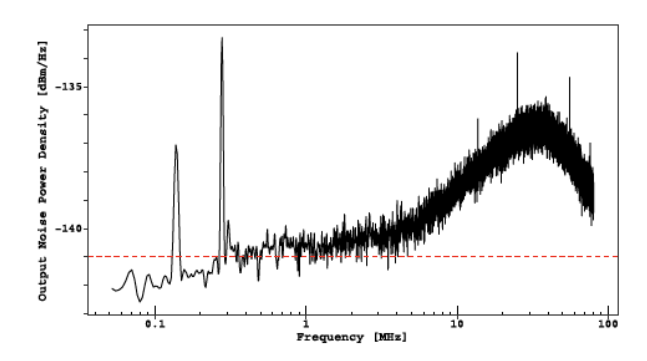


Fig. 11. Output noise density of the preamplifier discussed in the text at 77 K with the SiPM connected. Red line: analytical noise prediction.

C. Preamplifier Performance in Liquid Nitrogen

Values of $R_f=3.9~\mathrm{k}\Omega$ and $R_s=20~\Omega$ were selected to optimize the TIA performance at 77 K. With these values, the bandwidth of the preamplifier is always significantly higher than the fast rising edge of the SiPM (which is between 20 and 30 MHz and is extracted from the fit of the fast component of the waveform shown in Fig. 8).

Above F_l , the voltage noise at the input of the amplifier, $e_n^t(T) = (4 k_B T (R_n + R_+ + R_- + R_s + R_d))^{1/2}$, includes the intrinsic voltage noise of the LMH6629, e_n , and the Johnson–Nyquist noise of the other resistors in the circuit. In this formula, $R_n = 25 \Omega$ accounts for e_n , as described in Section II-C. In liquid nitrogen, $e_n^t(77 \text{ K}) = 0.7 \text{ nV}/\sqrt{\text{Hz}}$, corresponding to about -141 dBm/Hz at the output (taking into account the back termination of the output). The input current noise of the LMH6629, i_n , and the Johnson–Nyquist current noise of R_f together account for about 1.5 pA/ $\sqrt{\text{Hz}}$, which corresponds to about -157 dBm/Hz at the output and can therefore be ignored. Fig. 11 shows the output noise density spectrum of the preamplifier connected to the NUV-HD-LF $10 \times 10 \text{ mm}^2$ SiPM. The difference at 1 MHz between the prediction and the measurement is less than 1 dB.

The high-frequency bump present in the noise spectrum is due to the decrease of R_d at few MHz as described in Section III-A. With a vanishing R_d , the noise gain increases up to a theoretical factor of 4. In practice, this value is never reached due to the limited available GBP.

With a 4-V power supply, the preamplifier provides a dynamic range in excess of 250 photoelectrons with a power consumption of about 40 mW.

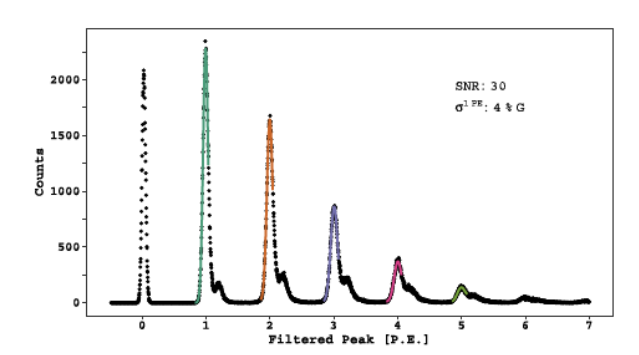


Fig. 12. Spectrum of photoelectrons after matched filtering for a 10×10 mm² NUV-HD-LF SiPM at 77 K.

D. Read-Out and Data Analysis

Cryogenic tests of the TIA with the $10 \times 10 - \text{mm}^2$ NUV-HD-LF SiPM were performed in the setup described in Section I. A Hamamatsu PLP-10 405-nm laser, capable of subnanosecond light pulses, was used as a light source. The signal from the TIA was fed out of the cryostat into a room temperature, low-noise amplifier and then digitized by a 10 bit, 2-GS/s CAEN V1751 configured with a pretrigger of 8 μ s and a total gate length of 15 μ s. The digitizer was triggered by the sync pulse of the PLP-10. The least significant bit of the digitizer is 1 mV, hence further amplification of the signal is required to avoid excessive quantization noise. A custom low-noise amplifier based on two THS3201 operational amplifiers [10] was built providing a bandwidth in excess of 200 MHz, a gain of 100 V/V, and an input noise density of about 1.6 nV/ $\sqrt{\text{Hz}}$.

Off-line analysis software was used to analyze the digitized waveforms and calculate the figures of merit. Of particular interest is the signal-to-noise ratio (SNR), defined as the ratio between the gain of the photoelectron peaks and the baseline noise. Two SNR parameters were calculated based on two different methods for calculating the charge of each waveform: the amplitude of the raw waveform at the peak (SNR $_{\rm r}$) and the amplitude of the digitally filtered waveform at the peak (SNR $_{\rm f}$). In both cases, the baseline noise was estimated as the standard deviation of the corresponding pretrigger raw or filtered waveform.

E. Matched Filter

The extraction of a signal with known shape from stochastic noise is maximized by the use of a matched filter [11]. Matched filtering is done by convolving the raw waveform with a time-reversed template waveform. The matched filter algorithm is implemented offline. For a given preamplifier configuration and temperature, the template waveform is determined by averaging baseline subtracted and time-aligned waveforms from single photoelectron events. The filtered waveform exhibits a symmetric shape around the photoelectron arrival time, where a peak is present. The identification of the charge and timing of the signal is performed by evaluating the amplitude and the timing of the filtered waveform maximum.

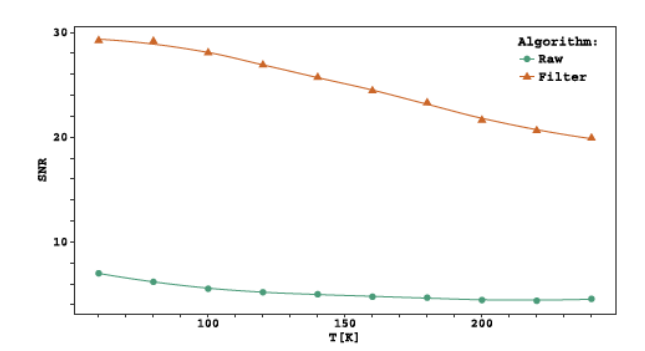


Fig. 13. Signal-to-noise figures as a function of temperature. The lines are drawn to guide the eye.

IV. RESULTS

The spectrum obtained using a $10 \times 10 - \text{mm}^2$ NUV-HD-LF SiPM at 77 K and the matched filter algorithm described in Section III-E, as shown in Fig. 12. An SNR of 30 is achieved with the SiPM operating at a gain of 1×10^6 C/C.

A. Signal Over Noise

Fig. 13 compares SNR_f and SNR_r as a function of temperature. The behavior of these curves includes many effects. To first order, both the signal amplitude and the baseline noise increase with higher temperature. A simple model that only considers the temperature dependence of the amplitude and the noise plateau over-predicts the decrease in SNR at room temperature. This is because the magnitude and shape of the output noise spectrum changes due to the temperature dependence of the TIA bandwidth, F_l , and F_p . The net effect on the baseline noise at the bandwidth of interest, which is also temperature dependent, is therefore difficult to model analytically.

B. Timing

The rise time of the unfiltered SiPM signal is a function of the amplifier bandwidth shown in Fig. 10 and is between 5 and 11 ns (modeling the rise time as 0.35/bandwidth). Given the relatively low SNR_r , a standard discriminator is not the best approach for determining the event timing. In situations like this, it is advantageous to use the entire SiPM waveform for event reconstruction. This is particularly true at cryogenic temperature when a large fraction of the total signal charge is contained in the slow recharge of the waveform. This is done using matched filtering, which preserves the fast component of the signal while maximizing the SNR and yielding nanosecond timing resolution. Fig. 14 shows the time jitter of the reconstructed event time relative to the laser pulse measured using the matched filtered waveform at 80 K. The standard deviation of the first photoelectron peak is 1.0 ns.

Fig. 15 shows the time distribution as a function of temperature for both filtered and unfiltered waveforms (in this case, using a simple threshold to define the timing). While the timing resolution of the filtered waveform is slightly affected by the temperature, the performance of the unfiltered waveform shows a strong degradation with temperature. This is expected because the jitter of a simple discrimination can

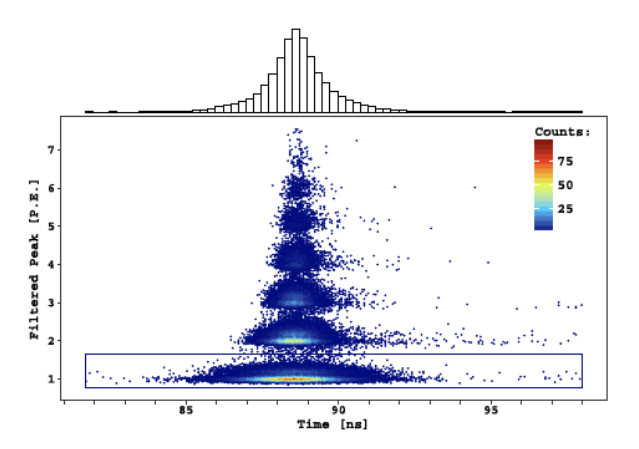


Fig. 14. Peak amplitude of the matched filtered waveform versus the reconstructed time relative to the laser sync at 80 K. The top histogram shows the timing distribution of the single photoelectron peak (within the black box). The standard deviation of the time is 1.0 ns.

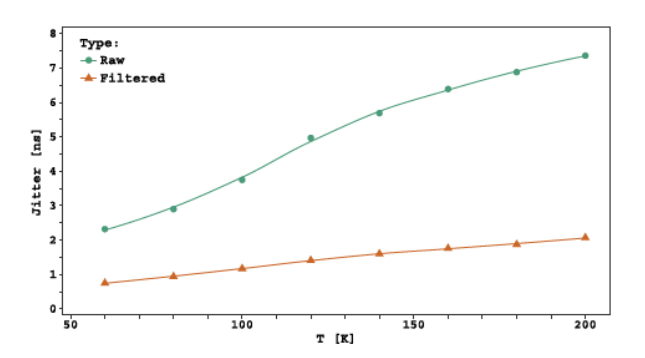


Fig. 15. Standard deviation of the calculated event time as a function of temperature for both matched filtered and raw waveforms. For the latter, a simple discriminator was used to determine the time of the event. The lines are drawn to guide the eye.

be quantified as the quotient of the rise time divided by the SNR. In our setup, the SNR decreases with temperature (see Fig. 13) and the bandwidth decreases with temperature (see Fig. 10), significantly reducing the fast rising edge of the waveform.

V. CONCLUSION

SiPM-based, cryogenic photodetectors with large active areas have great appeal for use in low-background particle physics experiments, where improvements in photodetection efficiency, resolution, and radio-purity directly impact experimental reach. The viability of such photodetectors relies on the development of cryogenic preamplifiers capable of preserving the fidelity of photon signals despite large sensor capacitance. In this paper, measurements of the electrical characteristics of a Texas Instruments LMH6629 were made over a range of temperatures from room temperature to 60 K and a cryogenic TIA was designed around the device. The resulting amplifier design was operated with a NUV-HD-LF, $10 \times 10 - \text{mm}^2$ SiPM with an SNR of 45 at 77 K when operating the SiPM at a gain of 1.5×6 C/C (5 V of overvoltage) and timing resolution better than 1 ns, thus demonstrating the practicality

of large-area SiPM detectors as conventional photomultiplier tube replacements for cryogenic applications.

REFERENCES

- F. Acerbi et al., "Cryogenic characterization of FBK HD near-UV sensitive SiPMs," IEEE Trans. Electron Devices, vol. 64, no. 2, pp. 521–526, Feb. 2017. [Online]. Available: http://ieeexplore.ieee.org/document/7807295/
 C. Aalseth et al. (2017). "DarkSide-20k: A 20 tonne two-phase LAr
- [2] C. Aalseth et al. (2017). "DarkSide-20k: A 20 tonne two-phase LAr TPC for direct dark matter detection at LNGS." [Online]. Available: https://arxiv.org/abs/1707.08145
- [3] W. P. Dumke, "The effect of base doping on the performance of Si bipolar transistors at low temperatures," *IEEE Trans. Electron Devices*, vol. ED-28, no. 5, pp. 494–500, May 1981. [Online]. Available: http://ieeexplore.ieee.org/document/1481524/
- [4] J. D. Cressler, "Operation of SiGe bipolar technology at cryogenic temperatures," J. Phys. IV France, vol. 04, no. C6, pp. C6-101–C6-110, 1994. [Online]. Available: http://www.edpsciences.org/10.1051/jp4: 1994616
- [5] "LMH6629 ultra-low noise, high-speed operational amplifier with shut-down," Texas Instrum., Dallas, TX, USA, Tech. Rep., 2016. [Online]. Available: www.ti.com/lit/ds/symlink/lmh6629.pdf

- [6] F. Teyssandier and D. Prêle, "Commercially available capacitors at cryogenic temperatures," in *Proc. WOLTE9*, 2010. [Online]. Available: https://hal.archives-ouvertes.fr/hal-00623399
- [7] C. Piemonte et al., "Performance of NUV-HD silicon photomultiplier technology," IEEE Trans. Electron Devices, vol. 63, no. 3, pp. 1111–1116, Mar. 2016. [Online]. Available: http://ieeexplore.ieee. org/lpdocs/epic03/wrapper.htm?arnumber=7397984
- [8] A. Ferri, F. Acerbi, A. Gola, G. Paternoster, C. Piemonte, and N. Zorzi, "Performance of FBK low-afterpulse NUV silicon photomultipliers for PET application," *J. Instrum.*, vol. 11, no. 3, p. P03023, 2016. [Online]. Available: http://stacks.iop.org/1748-0221/11/i=03/a=P03023? key=crossref.3b90668de68c0dbe8d723d4154a2ece8
- [9] D. Marano et al., "Silicon photomultipliers electrical model extensive analytical analysis," IEEE Trans. Nucl. Sci., vol. 61, no. 1, pp. 23–34, Feb. 2014. [Online]. Available: http://ieeexplore.ieee.org/document/6661445/
- [10] "1.8-GHz, low distortion, current-feedback amplifier," Texas Instrum., Dallas, TX, USA, Tech. Rep., 2003. [Online]. Available: http://www.ti.com/lit/ds/slos416c/slos416c.pdf
- [11] G. Turin, "An introduction to matched filters," *IRE Trans. Inf. Theory*, vol. 6, no. 3, pp. 311–329, Jun. 1960. [Online]. Available: http://ieeexplore.ieee.org/document/1057571/